

## Predictability of orbits in coupled systems through finite-time Lyapunov exponents

**Juan C Vallejo and Miguel A F Sanjuán**

Nonlinear Dynamics, Chaos and Complex Systems Group, Departamento de Física, Universidad Rey Juan Carlos, Tulipán s/n, E-28933 Móstoles, Madrid, Spain

E-mail: [juancarlos.vallejo@urjc.es](mailto:juancarlos.vallejo@urjc.es) and [miguel.sanjuan@urjc.es](mailto:miguel.sanjuan@urjc.es)

*New Journal of Physics* **15** (2013) 113064 (20pp)

Received 16 September 2013

Published 29 November 2013

Online at <http://www.njp.org/>

doi:10.1088/1367-2630/15/11/113064

**Abstract.** The predictability of an orbit is a key issue when a physical model has strong sensitivity to the initial conditions and it is solved numerically. How close the computed chaotic orbits are to the real orbits can be characterized by the shadowing properties of the system. The finite-time Lyapunov exponents distributions allow us to derive the shadowing timescales of a given system. In this paper we show how to obtain information about the predictability of the orbits even when using arbitrary initial orientation for the initial deviation vectors. As a model to test our results, we use a system of two coupled Rössler oscillators. We analyze the dependence of the shadowing time on the coupling strength and internal nature of the oscillators. The main focus rests on the dependence of these results on the length of the finite-time intervals and the computation of the most appropriate interval for a better forecast. We emphasize the importance of extracting information from all of the relevant exponents to obtain an insight into the sources of the nonhyperbolicity of the system.



Content from this work may be used under the terms of the [Creative Commons Attribution 3.0 licence](https://creativecommons.org/licenses/by/3.0/).

Any further distribution of this work must maintain attribution to the author(s) and the title of the work, journal citation and DOI.

**Contents**

<b>1. Introduction</b>	<b>2</b>
<b>2. Description of the model</b>	<b>3</b>
<b>3. Distributions of finite-time Lyapunov exponents</b>	<b>5</b>
<b>4. Hyperbolicity characterization</b>	<b>10</b>
<b>5. Shadowing</b>	<b>12</b>
<b>6. Predictability charts</b>	<b>13</b>
<b>7. Conclusions</b>	<b>17</b>
<b>Acknowledgments</b>	<b>18</b>
<b>References</b>	<b>18</b>

**1. Introduction**

In the last century, the numerical approach to solving physical problems has become more relevant with the increase of computational facilities. Methods derived from chaos theory and nonlinear dynamics techniques are quite useful in solving real problems where chaos is present and strong dependence on initial conditions is a key issue.

Predictability refers to the assessment of the likely errors in a forecast, either qualitatively or quantitatively. We can take a model, or set of equations describing the system, and integrate it during a certain time interval. How valid is the resulting forecast? Obviously, two initial points may diverge, or not, due to the presence of strong sensitivity to the initial conditions. The larger this sensitivity, the larger the likelihood that a computed orbit will diverge from the real one. A quantitative measure of this sensitivity is given by the computation of the Lyapunov exponents. The inverse of a Lyapunov exponent, sometimes called reliability time, provides a frequently used timescale for characterizing the reliability.

Note that even the best method will diverge from the true orbit beyond certain timescales. Certainly, this is due to the fact that all of the numerical calculations have inherent inaccuracies.

The shadowing property addresses this by characterizing for how much time a computed orbit is close to an actual orbit of the system. Numerically computed chaotic orbits may sometimes be sufficiently close to one true solution, called a shadow, leading to correct predictions. This can happen for chaotic, yet hyperbolic flows. Nevertheless, sometimes the shadowing property is only valid during very short times, as in the pseudo deterministic systems, when unstable dimension variability (UDV) [1] is the cause of the nonhyperbolicity. In these cases, the point may not be shadowed and the computed orbit may be far from the true one.

The shadowing times are of importance when modeling these systems and are a valid limit for the predictability of the system. The usage of any of the well known available chaoticity indicators (see [2] for a review) is sufficient if we are just interested in the chaotic or regular asymptotic global behavior of the system. But if we are interested in the predictability timescales of the system, the shadowing properties should be checked. These properties can be obtained from the statistical properties of the finite-time Lyapunov exponents distributions [3]. But these distributions strongly depend on the several available Lyapunov exponents, the finite interval lengths, and possible transient periods of the flow. We will analyze these dependences because we will use these distributions to derive the predictability of the system, even when the

finite intervals are much smaller than the intervals needed for reaching the asymptotic global Lyapunov exponent values.

The main goal of this paper is to analyze the predictability obtained from the distributions of finite-time Lyapunov exponents calculated using arbitrary initial deviation directions, when they are strongly dependant on the finite-time interval size [4]. Our motivation is derived from the fact that techniques based on finite-time Lyapunov exponents can be used in systems where asymptotic global results are not of interest, are not physically meaningful or even may not exist. We could be interested in the analysis of transient periods, which just exist for a while before the system reaches a final stationary state. Or it may happen that because of the physics of the system the timescales for obtaining the global properties are too long to be realistic, since the system nature may have evolved for such a period. For instance, similar Hamiltonian flows are used both in galactic dynamics and plasma physics but their dynamic timescales are rather different. Finally, we can deal with open systems where the orbits can escape, or chaotic scattering problems, where transient chaos may exist. Here, the indicators should be applied only during finite trapping times, before the particle gets out of the trapping area.

We focus our analysis on two coupled Rössler systems, a simple  $6D$  non-conservative dynamic flow which shows rich nonhyperbolic behavior. We track the complexity structure during the transitions from the hyperbolic to the nonhyperbolic regimes. We have obtained the shadowing properties of this system and characterized how good a computed orbit is compared to the real one. We have seen how this characterization depends on the length of the finite-time intervals and computed the most appropriate interval for a better forecast. We have also analyzed how the shadowing times vary as certain parameters and the coupling strengths of the system are modified.

The paper's structure is as follows. Section 2 introduces the model. Section 3 reviews the basic concepts of finite exponent distributions. We use those distributions in section 4 to obtain the hyperbolicity indicators which characterize the system. In section 5, we focus on the dependence of the hyperbolicity index on the used finite-time intervals. We provide the predictability charts of the flow and obtain some insight on the sources of nonhyperbolicity in section 6. Finally, some concluding remarks are made in section 7.

## 2. Description of the model

The model consists of two identical, symmetrically diffusively coupled Rössler systems. We wish to describe its behavior with the help of its global Lyapunov exponents. This system possesses paradigmatic behavior in relation to the chaos–hyperchaos transition and the UDV phenomenon, which was presented in [5, 6] in a very similar system. In addition, it is a quite meaningful physical system, as it may represent the selective diffusion of two species through a semi-permeable membrane in two continuously stirred tank reactors [7].

The equations of the system are

$$\begin{cases} \dot{x}_1 = -y_1 - z_1, \\ \dot{y}_1 = x_1 + ay_1, \\ \dot{z}_1 = b + z_1(x_1 - c) + d(z_2 - z_1), \\ \dot{x}_2 = -y_2 - z_2, \\ \dot{y}_2 = x_2 + ay_2, \\ \dot{z}_2 = b + z_2(x_2 - c) + d(z_1 - z_2). \end{cases} \quad (1)$$

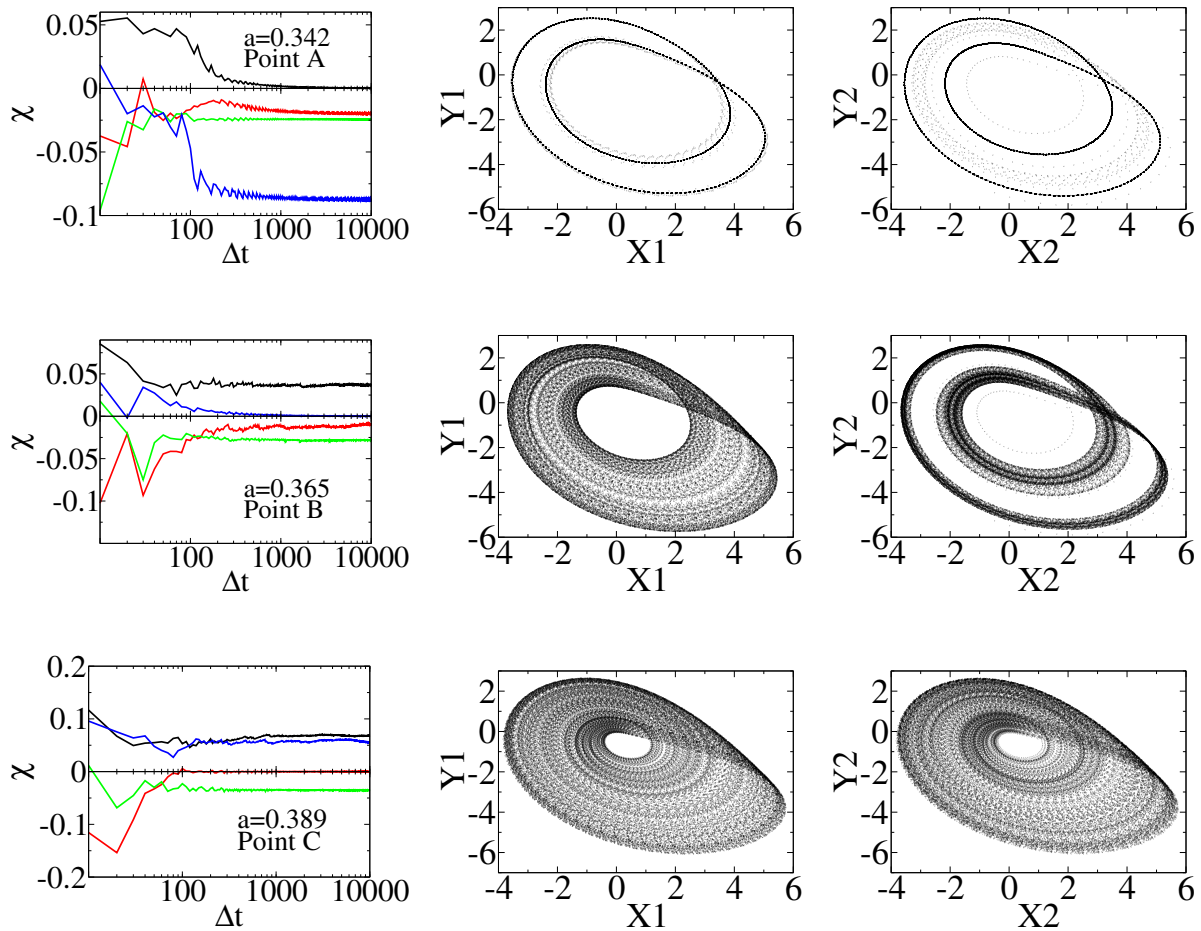


**Figure 1.** Evolution of the system of two coupled Rössler oscillators  $(x_1, y_1, z_1)$  and  $(x_2, y_2, z_2)$ . The leftmost column shows the convergence toward the global Lyapunov exponent of the four largest finite-time exponents from the total six available exponents. The remaining two exponents are always negative and do not provide additional information, so they are not displayed. The two rightmost columns show the values of  $(x_1, y_1)$  and  $(x_2, y_2)$ . The coordinates  $z_1$  and  $z_2$  are not shown, for simplicity. The total integration time is 10000 time units. A dot is plotted for every 0.1 time units. The coupling strength parameter is fixed as  $d = 0.25$ . Three values of the control parameter  $a$  are shown. The upper row corresponds to  $a = 0.342$ , the middle row to  $a = 0.365$  and the bottom row to  $a = 0.389$ . These three cases are indicated in figure 3 as A, B and C.

The first three coordinates  $(x_1, y_1, z_1)$  correspond to the first Rössler oscillator. The second three coordinates  $(x_2, y_2, z_2)$  to the other one. The parameter  $d$  represents the coupling, which depends on the distance between the  $z$ -coordinates of the oscillators. The parameter  $a$  is chosen as the control parameter. We have fixed parameters  $b = 2.0$  and  $c = 4.0$ , in order to compare our results with those from [5, 6]. We have used a simple fourth-order Runge–Kutta method, with fixed timestep 0.01 and a fourth-order/fifth-order Runge–Kutta–Fehlberg variable step size method as integration schemes, both leading to the same numerical results. Figure 1 shows the

evolution toward the final attractor of the oscillators. Note that only the  $(x_1, y_1)$  and  $(x_2, y_2)$  coordinates are displayed, the  $z$ -component being ignored. The plots are built with a total integration time of  $T = 10\,000$ , for three typical values of the control parameter  $a$ . The initial condition is  $(1, 1, 0, -1, -5, 0)$ , but the final attractor is the same in the neighborhood of this point. We see in this figure how the behavior for both oscillators is different as the parameter  $a$  changes. Different regimes for three values of  $a$  are reflected in the different convergence curves of the global Lyapunov exponents.

The global (also named ordinary or infinite) Lyapunov exponents describe the evolution in time of the distance between two nearly initial conditions, by averaging the exponential rate of divergence of the trajectories. It can be defined as

$$\lambda(\mathbf{x}, \mathbf{v}) = \lim_{t \rightarrow \infty} \frac{1}{t} \log_e \|D\phi(\mathbf{x}, t)\mathbf{v}\|, \quad (2)$$

provided this limit exists [8]. Here  $\phi(\mathbf{x}, t)$  denotes the solution of the flow of equation (1), such that  $\phi(\mathbf{x}_0, 0) = \mathbf{x}_0$ , and  $D$  means the spatial derivative in the direction of an infinitesimal displacement  $\mathbf{v}$ .

For  $N$ -dimensional flows, it is possible to have  $N$  global Lyapunov exponents when a distortion tensor formed from  $N$  perturbation vectors is evolved according to the flow equations. For a bounded orbit of an autonomous flow there is always an exponent with zero value in the limiting case (otherwise the system has an equilibrium in its limit set), as is tangent to the trajectory, and there is never any divergence for a perturbed trajectory in the direction of the unperturbed trajectory.

When considering a single Rössler system, the first exponent can be just zero or positive, the second exponent is zero and the third value negative, ensuring the boundness of the solution. When two oscillators are coupled, a richer set of values is present. The chaotic regime is defined when only one global Lyapunov exponent  $\lambda$  is positive, and the hyperchaotic regime, when more than one positive Lyapunov exponent is present.

The behavior of the global exponents and raising of hyperchaotic transition, as parameters  $a$  and  $d$  are varied, is shown in figure 2. In panel I, we fix coupling  $d = 0.25$  and vary  $a$ . Below  $a = 0.358$ , all of the exponents are either nearly zero or below zero. Above this number, we have the chaotic regime, where there is at least one exponent larger than zero. From  $a = 0.368$  there are at least two exponents, and the hyperchaotic regime starts. Note also that there is a window around  $a = 0.381$  where both of the exponents decrease toward zero. In panel II, we fix  $a = 0.358$  and vary  $d$ . For almost every coupling strength  $d$ , the system is hyperchaotic. However, there is a small interval around  $d \sim 0.174$ , where only the first global Lyapunov exponent remains positive. This shows that the chaos is not always decreasing (or increasing) with the coupling strength.

These different system regimes are displayed in figure 3, which shows the areas with no positive exponents (no chaos), just one positive exponent (chaos) and more than one positive exponent (hyperchaos). The hyperchaos arises in a complex way depending on the parameters  $a$  and  $d$ . There is no general trend of the hyperchaos with the coupling, as the chaos sometimes increases and sometimes decreases with coupling.

### 3. Distributions of finite-time Lyapunov exponents

The global Lyapunov exponents provide an indication of the globally averaged chaoticity of the system during an infinite integration time. But while they measure the asymptotic divergence of

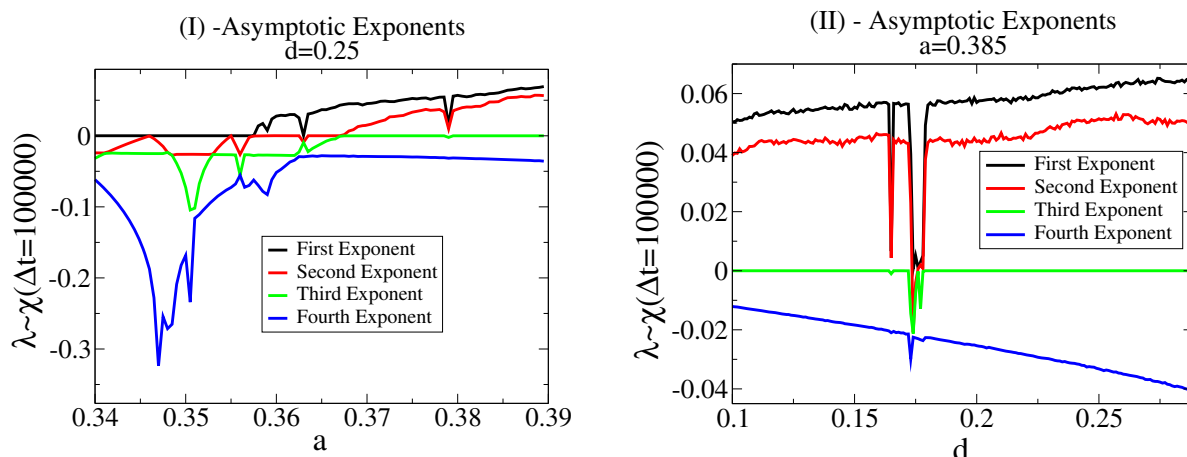


**Figure 2.** Lyapunov bifurcation diagrams. Only the four largest exponents from the total six are displayed. The remainder are always negative and are not shown. Global asymptotic Lyapunov exponent values  $\lambda$  are calculated by computing  $\chi(\Delta t = 100000)$ . Panel I shows the variation of  $\lambda$  with oscillator parameter  $a$  and fixed coupling strength  $d$ . Hyperchaos is born at around  $a \sim 0.367$ . Panel II shows the variation of  $\lambda$  with coupling strength  $d$  and fixed parameter  $a$ . There is a drop in the hyperchaotic regime at  $d \sim 0.174$ .

infinitesimally neighboring trajectories, it is not always possible or desirable to perform these very long integrations and the limit value. Indeed, sometimes the asymptotic limit, thus the exponents themselves, may not exist [8]. In this section, we review the concept of finite-time Lyapunov exponents, and their dependence on the interval length, initial orientation and total integration time. We will calculate their distributions along a single orbit and see how they characterize that orbit.

The standard definition of the Lyapunov exponent, equation (2), uses a very long (infinite) convergence time. Due to the sometimes slow convergence toward the asymptotic value, many other numerical indices and fast averaged indicators have been developed. We can cite, among others, the rotation index [9], the smaller alignment index [10] or its generalization, the generalized alignment index [11], the mean exponential growth factor of nearby orbits [12], the fast Lyapunov indicator [13], the relative Lyapunov indicator [14] or the finite-time rotation number [15].

The standard definition, however, still remains a valid indicator since it is quite easy to compute numerically. But, in practice, all of the numerically computed exponents are computed over finite-time intervals. Such values are generically named *finite* Lyapunov exponents. Unlike the global Lyapunov exponents, which take the same values for almost every initial condition in every region if chaoticity is sufficiently strong (except for a Lebesgue measure zero set, following the Oseledec theorem), the values of the exponents over finite times are generally different and may change in sign along one orbit.

We note here that there is a variety of notations and definitions regarding the finite-time Lyapunov exponents. For our purposes, we will focus on the following definition:

$$\chi(\mathbf{x}, \mathbf{v}, t) = \frac{1}{t} \log_e \|D\phi(\mathbf{x}, t)\mathbf{v}\|, \quad (3)$$

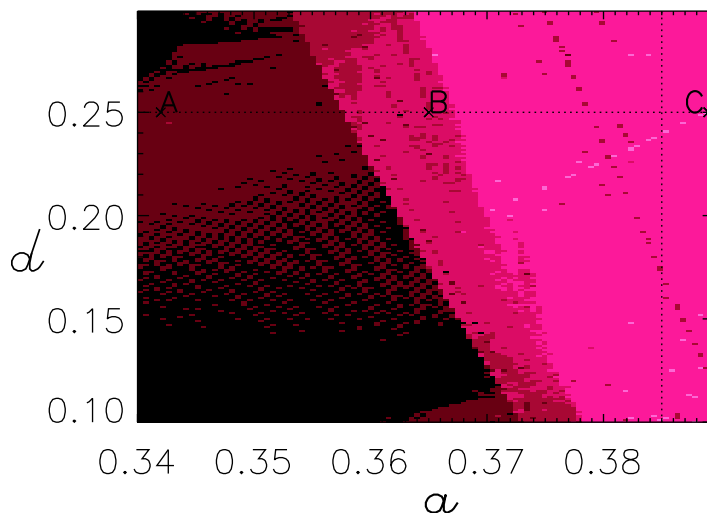


**Figure 3.** Hyperchaoticity chart. The number of positive global Lyapunov exponents varies with the Rössler parameter  $a$  and the coupling strength parameter  $d$ . Dark regions (black and dark red) mean zero positive exponents (dark red meaning that the convergence is slower). Mid-bright regions (red and dark pink) mean only one positive exponent (pink meaning slower convergence). Brighter regions (clear pink and above) mean two positive exponents. White means three. Slower convergence means that even with  $\Delta t = 100\,000$  the value has not reached the zero limiting case within machine precision, but it is already smaller than  $10^{-4}$ . Points A, B and C are the three plots of figure 1. Slicing horizontally at  $d = 0.25$  corresponds to figure 2 (top). Slicing vertically at  $a = 0.385$  corresponds to figure 2 (bottom).

which is derived from equation (2) for finite averaging times. Obviously,  $\lambda = \chi(\Delta t \rightarrow \infty)$ , with implicit dependence on the point  $\mathbf{x}$  and the deviation vector  $\mathbf{v}$ . This convergence toward the global asymptotic value is plotted in the leftmost column of figure 1. Note that only the four largest exponents of the total six available exponents are shown.

These exponents are generically labeled as *finite-time* Lyapunov exponents, independently of the finite interval length used in their computation. Notice that these exponents are sometimes named *effective* Lyapunov exponent for large but finite intervals [18], meanwhile the term *local* Lyapunov exponent is preferred when such an interval is small enough. The term *transient* Lyapunov exponent is found in [19], meaning intervals not large enough to ensure a satisfactory reduction of the fluctuations but small enough to reveal the slow trends. Finally, the *finite size* Lyapunov exponents [16] analyze the growth of the finite perturbations to a given trajectory, conversely to the analysis of the growth of infinitesimal perturbations performed by the finite-time exponents. For our purposes, we will use the generic *finite-time* Lyapunov exponents naming, independently of the length of the considered interval, and we will follow equation (3) for the exponent computations.

The finite-time Lyapunov exponents, computed according to equation (3), reflect the growth rate of the orthogonal semiaxes (equivalent to the initial deviation vectors) of one ellipse centered at the initial position as the system evolves. On fixing this initial point, there are several choices available for the initial orientation of the ellipse axes. Due to the dependence on the

finite integration time interval used in equation (3), every orientation will lead to different exponents [20]. One option is to have the axes pointing to the local expanding/contracting directions, given by the eigenvectors, and at local timescales the eigenvalues will provide insight into the stability of the point. Other options are the axes pointing to the direction which may have grown the most under the linearized dynamics, or pointing to the globally fastest growing direction. In what concerns this paper, the initial axes of the ellipse are set coincident with a random set of orthogonal vectors, as in [4].

We may perform the calculation by integrating two nearby trajectories, making them evolve under the flow dynamics and computing their distance, after being properly normalized, following the algorithm described in [21]. In our case, we have evolved the axes using the widely used variational method. We have solved, at the same time, the dynamic flow and the evolution of the  $6 - D$  distortion tensor (i.e. fundamental equation). The system of differential equations is then a 42-dimensional system, with the first six variables being  $(x_1, y_1, z_1, x_2, y_2, z_2)$  and the remaining 36 variables the components of six independent vectors, following each one of the variational equations. The growth rates of these ellipse axes will depend naturally on the flow timescales if we do not select any initial privileged direction. By solving the flow and the variational equations, we obtain the evolution in time of the infinitesimal vectors (variations) in every direction. An important issue when dealing with the finite integrations is the selection of the initial set of orthogonal vectors for solving the variational equation.

This algorithm returns the nearly asymptotic global Lyapunov values ordered from the largest to the smallest when large enough time intervals are used. Conversely, there will be just a linear relationship among the exponents when using very local timescales. But when using intermediate interval sizes, the main objective of this work, the returned values characterize a given orbit through the computation of their distribution functions or densities of probability.

If we make a partition of the whole integration time along one orbit into a series of time intervals of size  $\Delta t$  then it is possible to compute the finite-time Lyapunov exponent  $\chi(\Delta t)$  for every interval and plot its distribution. When normalized, dividing by the total number of intervals, we obtain a density function  $P(\chi)$  that gives the probability of obtaining a given value  $\chi$  between  $[\chi, \chi + d\chi]$ . We can obtain information about the degree of chaoticity of the orbit using these distributions, by subtracting the different spectra [22], deriving their power spectrum via the Fourier transform [23] or by analyzing their shapes and cumulants.

The finite-time Lyapunov exponents are named effective Lyapunov exponents when the intervals used to compute them are large enough, and the distributions can be analyzed from the cumulant generating function. This last function is defined as the logarithm of the moment generating function, which corresponds to the Fourier transform of the probability density function [18]. The first four cumulants are the mean, variance, skewness and kurtosis of the distributions, reflecting the deviation from a Gaussian curve. The *generalized* exponents are then associated with the order- $q$  moments of the distributions [17, 24].

We mention here a third factor affecting the distributions, in addition to the choice of the finite interval length and the initial directions of the axes. This is the total integration time used to compute the distribution [25]. Because the integration time for gathering the finite-time exponents is also finite, the distributions may just reflect any transient state of the system during such an integration period, instead of reflecting the global or final stationary state. The characterization of the orbit may change because of the slow convergence rate toward the asymptotic global value and the finite-time characterization of the orbit (hyperbolic or not) can change as the integration time changes [26, 27].

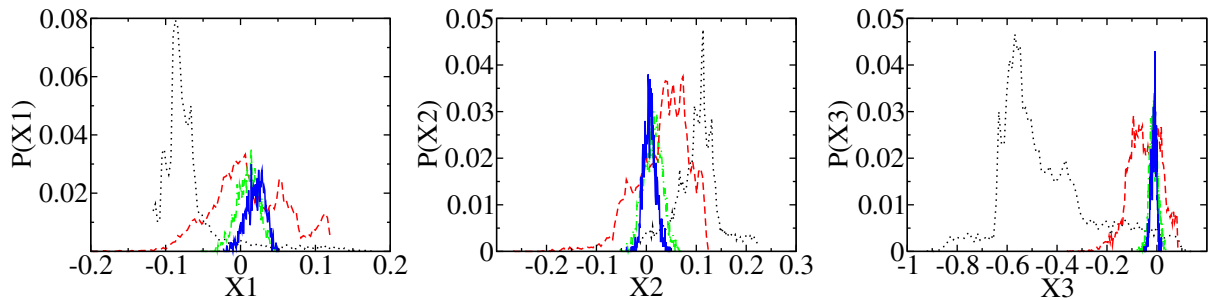


**Figure 4.** Density distributions  $P(\chi)$  for the first three finite-time exponents corresponding to point B of figure 3,  $a = 0.365$  and  $d = 0.25$ . These plots show how the center and the shape of the distributions depend on the finite interval length. As the finite interval  $\Delta t$  is increased, the distributions tend to shrink and center around the global Lyapunov exponent.  $\Delta t = 1.0$  is the black dotted line.  $\Delta t = 10.0$  is the red dashed line.  $\Delta t = 50.0$  is the green dot-dashed line.  $\Delta t = 100.0$  is the blue continuous line. The distributions sample a total integration time of  $T = 10\,000$  for all  $\Delta t$ , with the exception of  $T = 100\,000$ , when  $\Delta t = 100$  is analyzed. Table 1 contains the applicable numerical indices.

This means that in dissipative systems, one should take care of potentially existing transient periods within the used integration time before the final attractor is reached. Another obvious, yet important consequence of the selection of the total integration time used for building the distributions is that it must be long enough to provide enough data points for sampling and statistical analysis purposes.

We want to see these dependences because we will use the distributions to derive the predictability. We do not analyze here how  $\chi(\Delta t)$  tends to the value of  $\lambda$ , and how such an approximation is improved as the  $\Delta t$  interval is larger. Conversely, we focus here on analysing the distributions of the finite-time exponents  $\chi(\Delta t)$  computed with finite-time intervals, looking for the information those distributions provide on the system predictability.

The distributions corresponding to point B under hyperchaotic regime  $d = 0.25$  and  $a = 0.365$  of figure 3 are plotted in figure 4. This figure shows how the distribution shapes of the first three exponents depend on the finite interval length  $\Delta t$ . As  $\Delta t$  increases the distributions tend to shrink, being centered around the global Lyapunov exponent. The distributions sampled a total integration time of  $T = 10\,000$  for all  $\Delta t$ , with the exception of  $T = 100\,000$ , when  $\Delta t = 100$  is analyzed. The first integration time  $T = 10\,000$  is enough for proper display of the distributions and data analysis. Every curve contains a different but sufficient number of data points and the results are essentially the same as when using longer integration times. The case  $\Delta t = 100$ , however, requires the long integration  $T = 100\,000$ , in order to have enough data points and a reliable distribution. In table 1, we see this trend reflected as the evolution with  $\Delta t$  of the numerical indices associated with these distributions, the very small values of  $\sigma$  indicating the trend toward the asymptotic value.

The timescales necessary to orient the initial axes toward the final largest growth directions can be derived from observation of the evolution of the distributions. Actually, these timescales are different depending on the orbit nature. For very small timescales, there is a linear relationship among the exponents [4]. For larger timescales, the distributions can be used to

**Table 1.** Numerical indices associated with the finite-time Lyapunov exponent distributions corresponding to figure 4, for several  $\Delta t$  sizes. The standard deviation is  $\sigma$ . The probability of positivity  $F_+$ .

$\Delta t$	Mean	$\sigma$	$F_+$
$\chi_1$			
1.0	-0.065	0.046	0.079
10.0	0.013	0.051	0.55
50.0	0.010	0.015	0.73
100.0	0.021	0.013	0.93
$\chi_2$			
1.0	0.10	0.044	0.98
10.0	0.038	0.051	0.74
50.0	0.013	0.019	0.73
100.0	0.0071	0.012	0.71
$\chi_3$			
1.0	-0.44	0.19	0.028
10.0	-0.043	0.065	0.24
50.0	-0.013	0.017	0.21
100.0	-0.012	0.011	0.11

characterize the hyperbolic nature of the orbit. The tangencies among several directions can be seen as the linear dependences between the local exponents which are not lost for increasing timescales. The local eigenvolume evolution with time also gives us information to distinguish between chaotic and ordered orbits. For instance, the GALI-k index [11] is based on how the relationships among the different deviation vectors evolve. However, we are focusing on the predictability forecast derived from the distributions themselves.

#### 4. Hyperbolicity characterization

In this section, we discuss the possible nonhyperbolicity of the flow, because a basic requirement for shadowing is hyperbolicity. We also review the relationship of nonhyperbolicity and the finite-time exponent distributions.

A dynamic system is hyperbolic if the phase space can be spanned locally by a fixed number of independent stable and unstable directions which are consistent under the operation of the dynamics [3] and the angle between the stable and unstable manifolds is away from zero [28, 29]. Hyperbolic systems are *structurally* stable in the sense that the numerical trajectories stay close to the true ones. This phenomenon is called shadowing.

In case of nonhyperbolicity, an orbit may not be shadowed and the computed orbit behavior may be completely different from the true one. The nonhyperbolic behavior can arise from the tangencies between the stable and the unstable manifolds, from the UDV or from both.

When the nonhyperbolicity arises only from the tangencies, the trajectories may be still shadowed during long times. But in a general system, we could find unstable periodic orbits (UPO), KAM tori, KAM sticky orbits or chaotic sets. And in our system (dissipative), in addition to the tangencies, an attractor may pass very close to the periodic orbits with different

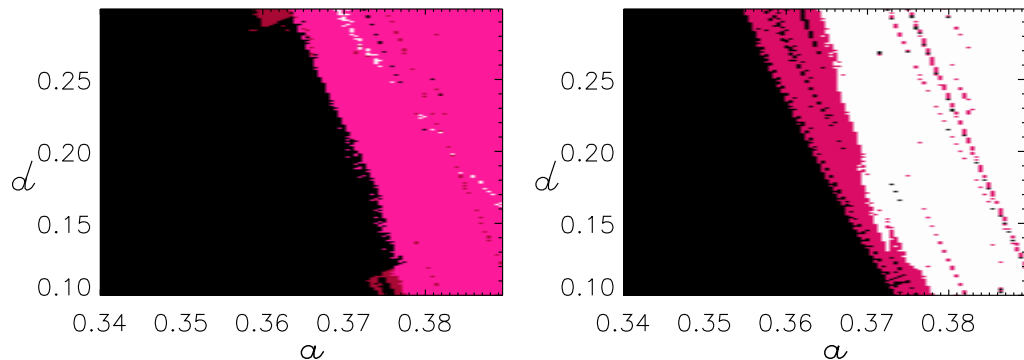


**Figure 5.** The identification of the exponent closest to zero varies with  $\Delta t$ , as derived from the mean of the probability density. Left:  $\Delta t = 25$  and  $T = 10\,000$ . When the exponent closest to zero is the first one we compute, it appears as black. If it is the second, it appears as red. If the third, it appears as pink. And, finally, for the fourth, it appears as white. Right:  $\Delta t = 100$  and  $T = 100\,000$ . In this case, the exponent closest to zero is only one of the three first exponents. If it is the first, it appears as black. If it is the second, it appears as red. And, finally, if it is the third, it appears as white.

number of unstable directions. This property of UPOs embedded in a chaotic invariant set is called UDV. In these pseudo deterministic systems, where the nonhyperbolicity arises from UDV, with or without the tangencies, the shadowing may be not good, meaning that the shadowing is only valid during trajectories of a given length, sometimes very short.

The UDV indicates a variation with position of the dimension of the invariant set subspaces, and is a major difficulty when modeling high-dimensional dynamic systems because the subspaces are not invariant along a typical chaotic trajectory. The UDV was first reported in the kicked double rotor, where the invariant set of interest is a chaotic attractor. Several mechanisms lead to the UDV, such as bubbling transitions in coupled oscillators, decoherence transitions in weakly coupled or non-identical systems and hyperchaos or extrinsic noise [30–33].

A sign of nonhyperbolicity and bad shadowing is then the fluctuating behavior around zero of the finite-time exponent closest to zero [34]. This reflects, in principle, the varying number of dimensions along the trajectory.

The exponent closest to zero can be derived from the inspection of the mean  $m$  of the distributions. The identification of the exponent closest to zero among all of the available exponents is helpful in characterizing the hyperbolicity, but varies with  $\Delta t$  (see figure 5). This is a consequence of the shape dependence of the distributions with the timescales.

For the smaller  $\Delta t$  intervals, these values have not evolved toward the final ordering. With  $\Delta t = 1.0$ , the directions have been already integrated 100 times, but the decorrelation has not yet taken place. For larger  $\Delta t$ , the distributions start to be Gaussian with a given mean centered around the global values. At  $\Delta t = 100.0$ , the mean of the distributions clearly tends to the global asymptotic values. As a consequence, the exponent closest to zero is the one tending to the neutral flow direction. Finally, when  $\Delta t \rightarrow \infty$  the distributions tend to be a Dirac delta function centered at the global asymptotic Lyapunov exponent value.

The oscillations of the exponent closest to zero can be detected when the positivity index  $F_+$  (equivalently, the probability of obtaining a positive  $\chi(\Delta t)$ )

$$F_+ = \int_0^{\infty} P(\chi) d\chi \quad (4)$$

is nearly 0.5.

How far are the positivity indices in the parameter space  $a - d$  from the 0.5 value? This proximity, or distance, is color coded in the leftmost column of figure 8, where darker regions are those with smaller values, meaning  $P_+ \sim 0.5$ . Conversely, the larger the values, the brighter the region and the farther from 0.5 in the positive or the negative directions. Areas of different behavior of the flow, such as the upper leftmost corner, with higher coupling strengths and smaller  $a$  control values, are identified even with the shorter intervals. The finest structures however can only be resolved with the larger intervals. Note that in different regions we have derived  $P_+$  from different closest to zero exponents, as this identification changes along the parametric phase space, as per figure 5.

We would like to emphasize that the exponents may fluctuate without being a clear cut of the UDV [35, 36]. There are situations where the positive tails appear not due to the UDV, but rather by other mechanisms such as the quasi-tangencies between the stable and unstable manifolds near a homoclinic crisis. Despite the above, the oscillations are still a good indication of the nonhyperbolic nature.

## 5. Shadowing

Our major goal is to characterize the predictability of an orbit by comparing the computed orbit with the real one, which is directly linked to the shadowing phenomenon. The computed distributions of the finite-time exponents provide detailed information on this. We are also interested in how this analysis depends on the chosen intervals to calculate these distributions.

The shadowing property characterizes the validity of long computer simulations, and how they may be *globally* sensitive to small errors. The shadowing time  $\tau$  measures how long a numerical trajectory remains valid by staying close to a true orbit. The shadowing distance is the local phase-space distance between the two.

When there is an oscillation of an exponent around zero, the shadowing distance typically mimics random walk behavior, swapping from exponential increases to decreases in the hyperbolic regions. This distance can also be described as the diffusion equation of a particle, which may find different escape routes along its trajectory. The larger shadowing times become improbable due to the diffusion processes.

This diffusion approximation assumes independent and identically distributed mean  $m$  and standard deviation  $\sigma$ . When we use the closest to zero exponent and assume both  $m$  and  $\sigma$  to be very small, the shadowing time  $\tau$  is given by [3]

$$\tau \sim \delta^{-h} \quad h = \frac{2\|m\|}{\sigma^2}, \quad (5)$$

where  $\delta$  is the round-off precision of the computer. The exponent  $h$  is called the hyperbolicity or predictability index. The worst case occurs when  $h$  is very small and there is no improvement in  $\tau$  even for large values of  $\delta$ . Conversely, the larger the  $h$  index, the better the shadowing.

We have computed equation (5) for several  $\Delta t$  intervals, even though equation (5) is only valid for ergodic distributions, with a Gaussian-like shape. This can be observed in figure 6.

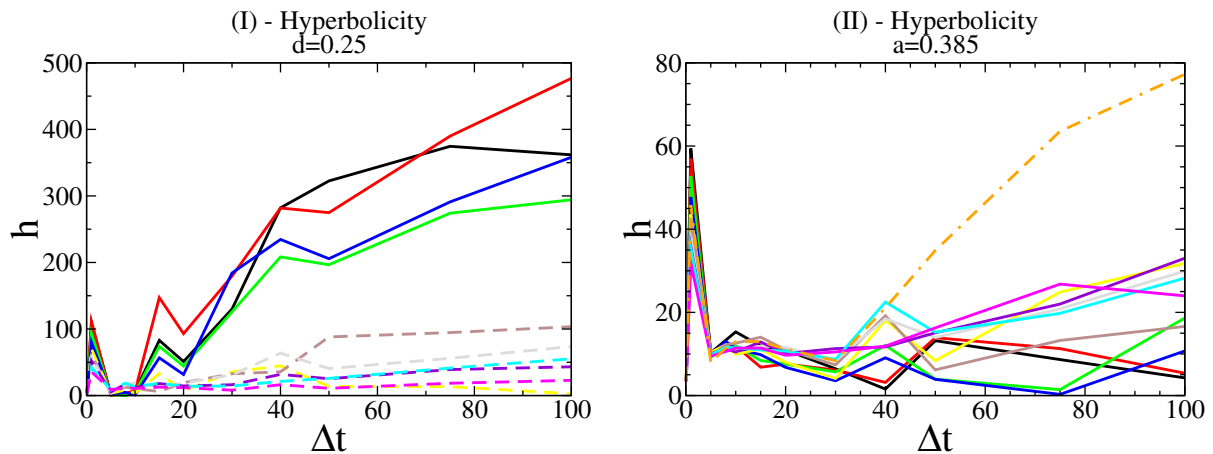


**Figure 6.** Hyperbolicity indices  $h$  calculated from the distributions of the closest to zero exponent, for different  $\Delta t$  intervals. Left: fixed coupling strength  $d$ . Calculations start at  $a = 0.34$ , every line increases  $a$  by 0.05 units. Continuous lines are  $a < 0.365$ . Dashed lines are those with  $a > 0.365$ . The regimes with low and high hyperbolicity are clearly identified, but only with a large enough  $\Delta t \sim 25$  interval. Right: fixed parameter  $a$ . Calculations start at  $d = 0.1$ , every line increases  $d$  by 0.02 units. Notice the dashed line  $d = 0.174$ , that is clearly separated from the remaining hyperchaotic cases with a large enough  $\Delta t \sim 50$  interval.

The leftmost diagram I of figure 6 plots the evolution of  $h(\Delta t)$  for a fixed value of  $d = 0.25$  and several  $a$  values. When  $\Delta t$  is small, the short finite times prevent the convergence of the exponents toward a limiting value. For this reason, the  $h$  values do not reach a final value and consequently they do not allow us to distinguish among different regimes. But as one can observe, for  $\Delta t$  values larger than 25, there are two main groups of curves  $h(\Delta t)$ . One upper set corresponds to the values  $a < 0.365$ , which corresponds to the non-chaotic regime, and is plotted as continuous lines. The lower set, in dashed curves, corresponds to  $a > 0.365$ , containing the chaotic and hyperchaotic regimes.

Similarly, the rightmost diagram II of figure 6 depicts the evolution of  $h$  with  $\Delta t$  for fixed  $a = 0.385$  and several  $d$  values. For almost every coupling strength  $d$ , the system can be considered hyperchaotic, implying low values of  $h$ . However, when  $d \sim 0.175$ , we find only one positive exponent, implying higher values of  $h$ . This can be clearly observed for  $\Delta t$  values larger than 40. In short, both graphs I and II indicate the dependence of the computed predictability not only on the combination of parameters  $a$  and  $d$ , but also on the size of  $\Delta t$ .

## 6. Predictability charts

Now we intend to establish the most appropriate interval length for the computation of the hyperbolicity index. The leftmost diagram I of figure 7 plots the evolution of  $h(a)$  for different values of  $\Delta t$ , with a fixed value  $d = 0.25$ . It can be clearly observed that the hyperbolicity index  $h$  decreases as  $a$  increases. The black continuous curve corresponds to the larger interval size  $\Delta t = 100$ . The red dashed curve is  $\Delta t = 50$  and the green dotted curve is  $\Delta t = 25$ . The larger

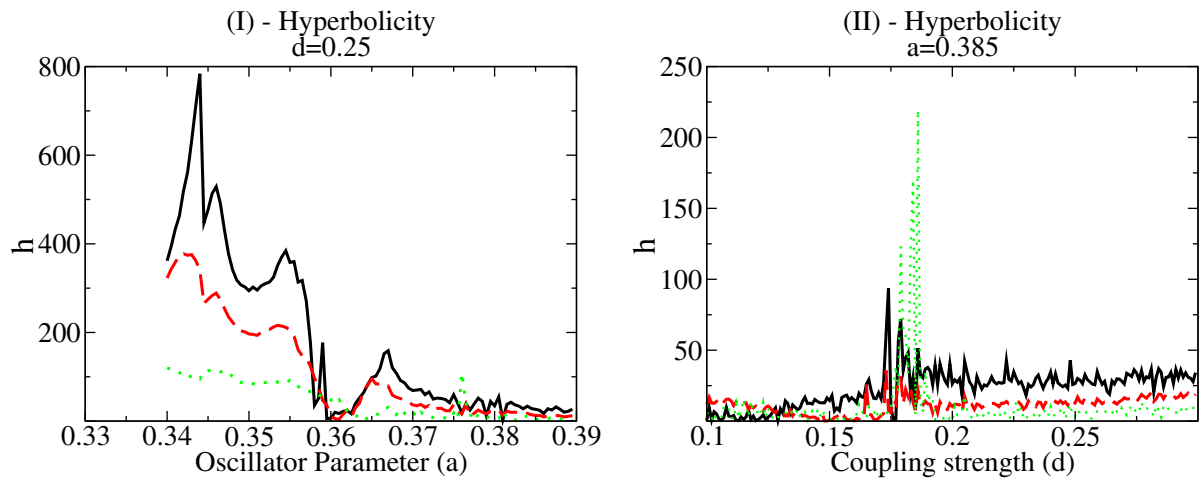


**Figure 7.** Hyperbolicity index  $h$  calculated from the distributions of the closest to zero exponent, for different  $\Delta t$  intervals. The black continuous curve is  $\Delta t = 100$ . The red dashed curve is  $\Delta t = 50$  and the green curve dotted is  $\Delta t = 25$ . Panel I: variation of  $h$  with  $a$ . Fixed coupling strength  $d = 0.25$ . The general trend of  $h$  decreasing with  $a$  is observed for all of the intervals, but the details are better seen with larger  $\Delta t$ . Panel II: variation of  $h$  with  $d$ . Fixed oscillator parameter  $a = 0.385$ . The high predictability peak at  $d \sim 0.17$  is better seen with the largest  $\Delta t$ .

the time interval  $\Delta t$ , the higher the detail in the observed structures. This is especially relevant for detecting the lowest predictability valley at around  $a = 0.36$ , which is coincident with the onset of the hyperchaotic regime. The rightmost diagram II of figure 7 plots  $h(d)$  with a fixed value  $a = 0.385$ , where we can see a roughly constant low predictability  $h$  for any coupling strength  $d$ . Interestingly, even at the smallest sizes of the intervals  $\Delta t$ , the high predictability peak is clearly detected in this almost hyperchaotic slice. In both figures, however, we can see that for  $\Delta t \sim 50$  or larger, the different regimes can be identified.

We want to extend the above results to the full parametric space  $a-d$ , and to see if there is a general pattern with the interval  $\Delta t$ . So we have plotted in figure 8, the rightmost column, the  $h$  index as derived from the closest to zero exponent in the full parametric space  $a-d$ , for different  $\Delta t$  values.

When using the smaller  $\Delta t$ , which in principle is associated with the less reliable  $h$  predictability values, there are still regions which are identified as having different predictability behavior. The plots of figure 7 are slices of the whole parametric space numerical explorations of figure 8, where we have identified different predictability zones even for the smaller intervals in certain areas of the parametric space. When inspecting the rightmost panels of figure 8, two main different behavior areas are clearly visible, as the available parametric space is divided into two behavior regions (left and right) from  $\Delta t = 25$  onwards. Indeed, some specific regions can be differentiated as having different behavior even at  $\Delta t = 1$ , although this identification is not very clear in this extreme case. This is the case of the upper-leftmost corner of the  $a-d$  diagram, corresponding to the higher coupling  $d$  and lower  $a$  values, identified as a region behaving differently from the others, with a very short decorrelation time, even with the shortest intervals. The other regions are however only clearly identified at larger  $\Delta t$ , when the distributions are

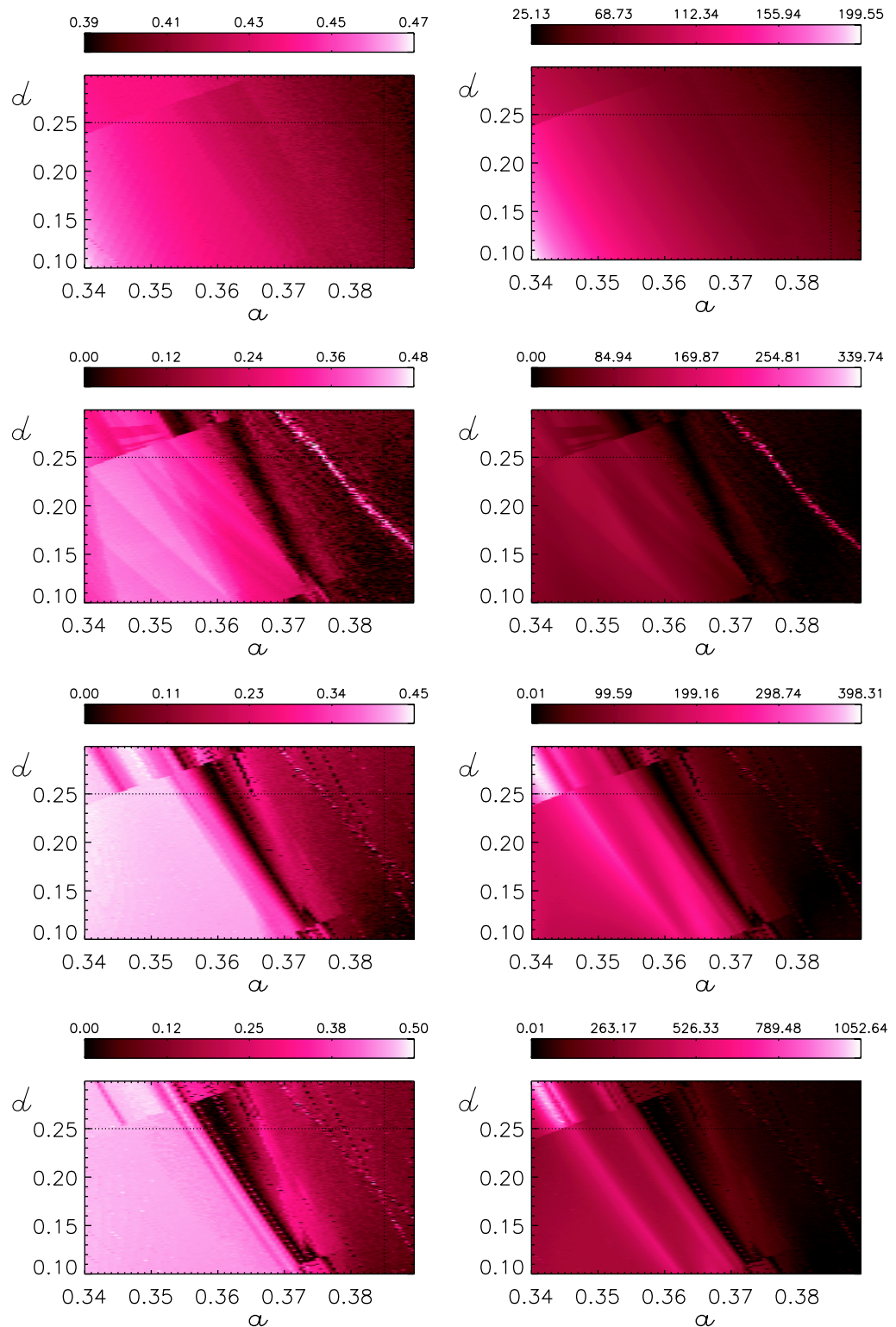


**Figure 8.** (Left column) Probability of positivity of the closest to zero exponent, for given oscillator parameter  $a$  and coupling strength  $d$ . Scaled values give the distance to  $P_+ = 0.5$ . Darker areas, values near to 0.0, are those with smaller values and  $P_+ \sim 0.5$ . This means the distributions centered around zero

**Figure 8.** (Continued) (stretched or shrunk). Brighter areas with larger values are farther from 0.5 in the positive or the negative direction. (Right column) Predictability chart, or  $h$  index derived from the closest to zero exponent, for given  $a$  and  $d$ . Darker values reflect  $h$  lower and mean poor predictability. From top to bottom,  $\Delta t = 1$  and  $T = 10\,000$ ,  $\Delta t = 25$  and  $T = 10\,000$ ,  $\Delta t = 50$  and  $T = 100\,000$  and  $\Delta t = 100$  and  $T = 100\,000$ .

nearly Gaussian, and both  $m$  and  $\sigma$  are small enough. This means that the decorrelation time for reaching a Gaussian-like shape and reliable  $h$  indices varies with the  $a$ - $d$  values. Some of the regions are easily identified as having different predictability behavior for shorter  $\Delta t$  values from other regions, where larger  $\Delta t$  are needed.

We have focused on finding the interval sizes for detecting the nonhyperbolic cases of worst predictability. But we can get some additional insight into the sources of the nonhyperbolicity by comparing the predictability  $h$  charts with the positivity charts and the hyperchaoticity charts.

The nonhyperbolicity can arise from the tangencies between the stable and the unstable manifolds, from the UDV or from both. When the UDV is present, the shadowing times can be very short with oscillations around zero of the closest to zero exponent present. We compare in figure 8 the predictability  $h$  charts with the positivity charts, as the latter reflect the around-zero oscillations of the closest to zero exponent. This comparison may provide a clue to the role of the UDV in the loss of predictability. As the starting point, our system is very close to the one shown in [5, 6], where the UDV was reported to be present. So the UDV is probably the source for the nonhyperbolicity, at least in the cases of worst predictability (smaller shadowing times). In figure 8, we see that there is good agreement among the darkest areas of both figures, mainly the central part, where both  $P_+ \sim 0.5$  and  $h$  are low. Now, we should be aware that at the largest intervals, the  $P_+$  is not properly detected, as the distributions are tending toward the asymptotic global value. Again,  $\Delta t \sim 25$  seems to be an adequate range for comparison. Some of the regions of different behavior, such as the one conforming to the right part of the parametric space, are nevertheless detected with almost every  $\Delta t$  interval. In this region, we obtain low predictability  $h$ , but there are no large oscillations around zero, as reflected in how  $P_+$  deviates from 0.5.

Hyperchaos is a common source for the UDV. When comparing the worst predictability areas, or darker areas in the rightmost column of figure 8, with the high chaotic areas of figure 3, we see the darker zones roughly match with the hyperchaos areas of figure 3. However, the match is not perfect, and here we may conjecture that the UDV is not fully sourced to the hyperchaos here. Conversely, no area of high chaoticity matches with a high predictability area. When comparing the high predictability areas, or brighter areas in the rightmost column of figure 8, with the less chaotic areas of figure 3 (those with none or just one single positive exponent) we note that they are similar, but not identical. This means that not all of the well-behaved areas have the same order of predictability. As discussed previously, these comparisons are best when using the largest  $\Delta t$ . But even at  $\Delta t \sim 25$  or even less, the chart can be of interest.

## 7. Conclusions

We have computed the hyperbolicity index of a system formed by two coupled Rössler oscillators, by using finite-time Lyapunov exponent distributions. We wish to stress the importance of computing the predictability of a system besides its possible chaotic behavior. A system can be chaotic, yet predictable (i.e. have long shadowing times). Conversely, a chaotic system can have poor predictability, understood as having low shadowing times. This predictability is linked to the structural sensitivity of the system and the validity of potential long computer simulations. Most chaoticity indicators are *global* or *averaged*. Independently of their convergence efficiency, they average along a given integration time, which might be larger or shorter depending on the convergence rate. When the shadowing times are short, these averaged quantities should be handled with care, and the shadowing times themselves may be used as limits for the averaging times.

The predictability is derived from the finite-time Lyapunov exponent distributions. As a consequence, we have noticed the importance of the choice of the finite interval  $\Delta t$ , because the distribution shapes depend on  $\Delta t$ , provided an adequate total sampling time. The analysis of the appropriate  $\Delta t$  allows us to choose the most suitable integration scheme, taking into account errors in the initial condition or machine truncation errors. The timescales derived from the value of the hyperbolicity index  $h$  are of help to make such a choice.

When the finite-time Lyapunov exponents are computed with an initial random orientation of the ellipse axes, we obtain different hyperbolicity indices depending on the finite interval length, since their distributions depend on the correlation times. In [4], we show how  $h$  varies with the different orbit types when computed with finite-time Lyapunov exponent distributions using very short intervals, where the typical timescale is of the order of the Poincaré crossing time. Here, we have derived  $h$  from the time intervals providing a Gaussian like density distribution, thus a reliable  $h$  computation.

In addition to the known fact that the more you integrate the better you can estimate the asymptotic Lyapunov exponent, we have also seen that using finite-time distributions and very short time intervals is sufficient for distinguishing the regions of different predictability behavior. This can be explained because the shapes reflect in detail the local flow of the system at these very short time intervals. We note here that the effective Lyapunov exponents can trace the stable and the unstable manifolds (the latter with a time backwards integration) [26, 37, 38]. In turn, the angle between both of the manifolds also gives information about the nonhyperbolic nature of the system, which is the main subject of this paper.

Our results are obtained for a 6D system, and stress the importance of calculating all of the exponents. The nonhyperbolic nature of the flow is related to the existence of tangencies between the stable and the unstable manifolds, from the UDV or from both. And we have seen that hyperchaos is a common source of UDV. When the manifolds are multidimensional, the analysis of all of the exponents is needed. The same can be said for detecting the hyperchaos strength. In addition to that, once all of the exponents are computed, we get an indication of two different timescales in the dynamics when the first positive exponent is much larger than the second positive exponent.

The presence of the oscillations of the closest to zero exponent is an indicator of nonhyperbolicity. This implies the necessity of the calculation of several available exponents, as the identification of the closest one depends on the selected interval, in addition to the position in the parametric space. We have noticed that for the larger intervals the exponents tend to the

global values, the closest to the zero points to the neutral direction and the oscillations may be then difficult of being clearly identified.

In general, the coupling between the two oscillators simply leads to their synchronization. However, there are cases where the coupling can lead to the inhibition of synchronization, anomalous phase synchronization or even amplitude death [39]. The study on how the synchronization of the two oscillators changes with the combination of  $a$  and  $d$ , and the relationship with their chaoticity is an interesting topic to extend the results of our work.

Our methods derive from calculating the distributions during certain integration times  $T$  of the finite exponents. This method does not use global averaged quantities during long intervals, unless strictly needed. So it can be used for open systems where transient chaos is found, taking care that the total integration time required for extracting information of the distribution is smaller than the trapping time. Here we note that the hyperbolic regime in the open systems shows an exponential decay law, meanwhile in the nonhyperbolic one, because of the KAM tori, there is an algebraic decay because of stickiness [40].

Finally, the identification of areas with low predictability is of interest when applying controlling chaos methods. Many control methods are based on the identification of UPOs and how the orbit is pushed first toward the stable manifolds, then toward the unstable, manifolds the based on the Ott–Grebogi–Yorke method (OGY), first described in [41]. By applying carefully chosen control impulses, it should be possible to carry the actual orbit toward the stable manifold. However, in the regions with tangencies, such an approach could be taken with care. Methods based on synchronization could also be affected by the different hyperbolicity indices due to the dependence on the coupling strength of the oscillators.

## Acknowledgments

This work was financed by the Spanish Ministry of Science and Innovation under project number FIS2009-09898.

## References

- [1] Abraham R and Smale S 1970 Non-genericity of  $\Omega$ -stability *Proc. Symp. Pure Math. Am. Math. Soc.* **14** 5
- [2] Skokos Ch 2010 The Lyapunov characteristic exponents and their computation *Lecture Notes Phys.* **790** 63–135
- [3] Sauer T, Grebogi C and Yorke J A 1997 How long do numerical chaotic solutions remain valid? *Phys. Lett. A* **79** 59
- [4] Vallejo J C, Viana R and Sanjuan M A F 2008 Local predictability and non hyperbolicity through finite Lyapunov exponents distributions in two-degrees-of-freedom Hamiltonian systems *Phys. Rev. E* **78** 066204
- [5] Yanchuk S and Kapitaniak T 2001 Symmetry increasing bifurcation as a predictor of chaos–hyperchaos transition in coupled systems *Phys. Rev. E* **64** 056235
- [6] Yanchuk S and Kapitaniak T 2001 Chaos–hyperchaos transition in coupled Rössler systems *Phys. Lett. A* **290** 139
- [7] Mosekilde E 1996 *Topics in Nonlinear Dynamics: Applications to Physics, Biology and Economics* (Singapore: World Scientific)
- [8] Ott W and Yorke J A 2008 When Lyapunov exponents fail to exist *Phys. Rev. E* **78** 056203
- [9] Voglis N, Contopoulos G and Efthymiopoulos C 1999 Detection of ordered and chaotic orbits using the dynamical spectra *Celest. Mech. Dyn. Astron.* **73** 211

- [10] Skokos Ch 2001 Alignment indices: a new, simple method for determining the ordered or chaotic nature of orbits *J. Phys. A: Math. Gen.* **34** 10029
- [11] Skokos Ch, Bountis T C and Antonopoulos Ch 2007 Geometrical properties of local dynamics in Hamiltonian systems: the generalized alignment index (GALI) method *Physica D* **231** 30
- [12] Cincotta P M and Simo C 2000 Simple tools to study global dynamics in non-axisymmetric galactic potentials *Astron. Astrophys. Suppl.* **147** 205
- [13] Froeschle C and Lega E 2000 On the structure of symplectic mappings. The fast Lyapunov indicator: a very sensitivity tool *Celest. Mech. Dyn. Astron.* **78** 167
- [14] Sandor Zs, Erdi B, Szell A and Funk B 2004 The relative Lyapunov indicator. An efficient method of chaos detection *Celest. Mech. Dyn. Astron.* **90** 127
- [15] Szezech J D Jr, Schelin A B, Caldas I L, Lopes S R, Morrison P J and Viana R L 2013 Finite-time rotation number: a fast indicator for chaotic dynamical structures *Phys. Lett. A* **377** 452
- [16] Boffetta G, Cencini M, Falcioni M and Vulpiani A 2002 Predictability: a way to characterize complexity *Phys. Rep.* **356** 367
- [17] Badii R, Heinzelmann K, Meier P F and Politi A 1988 Correlation functions and generalized Lyapunov exponents *Phys. Rev. A* **37** 1323
- [18] Grassberger P, Badii R and Politi A 1988 Scaling laws for invariant measures on hyperbolic and non-hyperbolic attractors *J. Stat. Phys.* **51** 135
- [19] Kapitaniak T 1993 Generating a strange nonchaotic trajectory *Phys. Rev. E* **47** 1408
- [20] Ziehmann C, Smith L A and Kurths J 2000 Localized Lyapunov exponents and the prediction of predictability *Phys. Lett. A* **271** 237
- [21] Benettin G, Galgani L and Strelcyn J M 1976 Kolmogorov entropy and numerical experiments *Phys. Rev. A* **14** 2338
- [22] Voglis N, Contopoulos G and Efthymiopoulos C 1998 Method for distinguishing between ordered and chaotic orbits in four-dimensional maps *Phys. Rev. E* **57** 372
- [23] Vozikis Ch L, Vavrogli H and Tsiganis K 2000 The power spectrum of geodesic divergences as an early detector of chaotic motion *Astron. Astrophys.* **359** 386
- [24] Crisanti A, Paladin G and Vulpiani A 1993 *Product of Random Matrices (Series in Solid State Sciences vol 104)* ed P Fulde (Berlin: Springer) pp 22–9
- [25] Vallejo J C, Aguirre J and Sanjuan M A F 2003 Characterization of the local instability in the Henon–Heiles Hamiltonian *Phys. Lett. A* **311** 26
- [26] Branicki M and Wiggings S 2010 Finite-time Lagrangian transport analysis: stable and unstable manifolds of hyperbolic trajectories and finite-time exponents *Nonlin. Proc. Geophys.* **17** 1
- [27] Mancho A M, Wiggins S, Curbelo J and Mendoza C 2013 Lagrangian descriptors: a method for revealing phase space structures of general time dependent dynamical systems *Commun. Nonlinear Sci.* **18** 3530
- [28] Viana R L and Grebogi C 2000 Unstable dimension variability and synchronization of chaotic systems *Phys. Rev. E* **62** 462
- [29] Kantz H, Grebogi C, Prasad A, Lai Y C and Sinde E 2002 Unexpected robustness-against-noise of a class of nonhyperbolic chaotic attractors *Phys. Rev. E* **65** 026209
- [30] Viana R L, Pinto S E, Barbosa J R and Grebogi C 2003 Pseudo-deterministic chaotic systems *Int. J. Bifurcation Chaos Appl. Sci. Eng.* **11** 1
- [31] Sauer T D 2002 Chaotic itinerancy based on attractors of one-dimensional maps *Phys. Rev. E* **65** 036220
- [32] Sauer T D 2003 *Chaos* **13** 947
- [33] Barreto E and So P 2000 Mechanisms for the development of unstable dimension variability and the breakdown of shadowing in coupled chaotic systems *Phys. Rev. Lett.* **85** 2490
- [34] Davidchack R L and Lai Y C 2000 Characterization of transition to chaos with multiple positive Lyapunov exponents by unstable periodic orbits *Phys. Lett. A* **270** 308
- [35] Viana R L, Barbosa J R, Grebogi C and Batista A M 2005 Simulating a chaotic process *Braz. J. Phys.* **35** 1

- [36] Alligood K T, Sander E and Yorke J A 2006 Three-dimensional crisis: crossing bifurcations and unstable dimension variability *Phys. Rev. Lett.* **96** 244103
- [37] Doerner R, Hubinger B, Martiensen W, Grossmann S and Thomae S 1999 Stable manifolds and predictability of dynamical systems *Chaos Solitons Fractals* **10** 1759
- [38] Haller G 2000 Finding finite-time invariant manifolds in two-dimensional velocity fields *Chaos* **10** 99
- [39] Resmi V, Ambika G and Amritkar R E 2011 General mechanism for amplitude death in coupled systems *Phys. Rev. E* **84** 046212
- [40] Seoane J and Sanjuan M A F 2010 Escaping dynamics in presence of dissipation and noise in scattering systems *Int. J. Bifurcation Chaos* **20** 2783
- [41] Ott E, Grebogi C and Yorke J A 1990 Controlling chaos *Phys. Rev. Lett.* **64** 1196

Copyright of New Journal of Physics is the property of IOP Publishing and its content may not be copied or emailed to multiple sites or posted to a listserv without the copyright holder's express written permission. However, users may print, download, or email articles for individual use.